YALE PEABODY MUSEUM

JOURNAL OF MARINE RESEARCH

The *Journal of Marine Research,* one of the oldest journals in American marine science, published important peer-reviewed original research on a broad array of topics in physical, biological, and chemical oceanography vital to the academic oceanographic community in the long and rich tradition of the Sears Foundation for Marine Research at Yale University.

An archive of all issues from 1937 to 2021 (Volume 1–79) are available through EliScholar, a digital platform for scholarly publishing provided by Yale University Library at https://elischolar.library.yale.edu/.

Requests for permission to clear rights for use of this content should be directed to the authors, their estates, or other representatives. The *Journal of Marine Research* has no contact information beyond the affiliations listed in the published articles. We ask that you provide attribution to the *Journal of Marine Research.*

Yale University provides access to these materials for educational and research purposes only. Copyright or other proprietary rights to content contained in this document may be held by individuals or entities other than, or in addition to, Yale University. You are solely responsible for determining the ownership of the copyright, and for obtaining permission for your intended use. Yale University makes no warranty that your distribution, reproduction, or other use of these materials will not infringe the rights of third parties.

Journal of

MARINE RESEARCH

On the differences between bubble-mediated air-water transfer in freshwater and seawater

by W. E. Asher[1,2], L. M. Karle[1,3] and B. J. Higgins[1,4]

ABSTRACT

Bubble populations and gas transfer velocities were measured in cleaned and surfactant-influenced freshwater and seawater. A nonlinear fitting technique was used to partition the total gas transfer velocity for a gas in each water type into a turbulence- and bubble-mediated fraction. This showed that the bubble-mediated transfer fraction was larger in cleaned freshwater than in cleaned seawater and that the difference was a function of diffusivity and solubility. This was explained by the fact that the bubble measurements showed that bubble plumes in cleaned freshwater had a higher concentration of large bubbles and a lower concentration of small bubbles than the plumes in cleaned seawater. The differences between the behavior of the bubble-mediated gas flux in cleaned freshwater and cleaned seawater show that caution should be used when intercomparing laboratory results from measurements made in different media. These differences also will make parameterizations of bubble-mediated gas exchange developed using freshwater laboratory data difficult to apply directly to oceanic conditions. It was found that adding a surfactant to seawater had minimal impact on the concentration of bubbles in the plumes. Because surfactants decrease the gas flux to the individual bubbles, the similarity in bubble population meant that the addition of surfactant to seawater decreased the bubble-mediated gas flux compared to the flux in cleaned seawater. In contrast, the addition of a surfactant to freshwater increased the concentration of bubbles by over an order of magnitude. This increase in bubble population was large enough to offset the decrease in the flux to the individual bubbles so that the net bubble-mediated gas flux in freshwater increased when surfactant was added. This difference in behavior of the bubble population and bubble-mediated

1. Pacific Northwest National Laboratory, 1529 W. Sequim Bay Road, Sequim, Washington, 98382, U.S.A.
2. Present address: Applied Physics Laboratory, University of Washington, 1013 NE 40th Street, Seattle, Washington, 98105, U.S.A.
3. Present address: Immunex Corporation, 51 University Street, Seattle, Washington, 98101, U.S.A.
4. Present address: Anteon Corporation, at the US Army Corps of Engineers, Seattle, Washington, 98124, U.S.A.

transfer velocity between surfactant-influenced and cleaned waters further complicates interrelating laboratory measurements and applying laboratory results to the ocean.

1. Introduction

Air-water gas transfer is an important process in marine and freshwater systems. The net air-water flux, F, of a sparingly soluble gas is usually calculated as the product of the air-water concentration difference, ΔC, and the air-water transfer velocity, k_L. It is relatively simple to determine ΔC for a variety of gases in natural waters. In contrast, direct measurements of k_L are available only for a limited suite of reference tracer species. Transfer velocities for other gases of interest must be estimated from the reference k_L values based on similarity of the physical forcing functions and an assumed dependence of k_L on the physico-chemical properties of the gas-water system. In support of earlier modeling studies (Memery and Merlivat, 1985; Woolf and Thorpe, 1991; Keeling, 1993; Woolf, 1993; Woolf, 1997), the laboratory measurements by Asher et al. (1996) showed that bubble-mediated transfer affects the dependence of k_L on diffusivity and solubility. Because assuming an incorrect functional form for this dependence can lead to significant errors in the estimated k_L value (Asher and Wanninkhof, 1997), it is important to know how to parameterize k_L in the presence of bubbles.

Modeling studies have shown that changes in the size distribution and concentration of the bubble population can affect bubble-mediated air-water gas transfer velocities (Keeling, 1993; Woolf, 1993). Keeling (1993) has also shown that the bubble population affects the dependence of k_L on the physical and chemical constants. Furthermore, there are significant differences in the size distribution of the bubble population between freshwater and seawater (Shatkay and Ronen, 1992; Haines and Johnson, 1995; Wanninkhof et al., 1995). Therefore, there also could be differences in the bubble-mediated transfer process.

Previous studies of bubble-driven gas transfer have used wind tunnels (Broecker and Siems, 1984; Jähne et al., 1984), surf pools (Asher et al., 1995), and whitecap simulation tanks (Asher et al., 1996). The corrosiveness of seawater precludes its use in the larger facilities, so most of the wind tunnel and surf pool data have been collected in freshwater. If there are significant differences between bubble transfer in freshwater and seawater, application of parameterizations for k_L developed using freshwater data to seawater might result in erroneous values for the gas flux. Unfortunately, it is difficult to assess how large an effect this change in salinity could have on the functionality of k_L. Gas transfer measurements made in freshwater and seawater for known bubble populations could be used to determine how the functionality of k_L changes between the two media.

In the absence of bubbles, models and experiments have shown that at constant levels of turbulence, k_L can be written as

$$k_L = A(v/D)^{-n} \tag{1}$$

where A is a turbulence-dependent constant, v is the kinematic viscosity of water, D is the diffusivity of the gas, the exponent n lies in the range $\frac{1}{2} \leq n \leq \frac{2}{3}$ depending on the

cleanliness of the water surface, and the ratio v/D is referred to as the Schmidt number, Sc, of the gas.

The use of (1) makes interrelating k_L values for any two gases simple if the bubble-mediated gas flux is negligible. However, as mentioned above k_L is a function of both D and the aqueous-phase solubility of the gas, α (i.e., the nondimensional Ostwald solubility (Reid *et al.* (1987)) when bubbles are present. The dependence of k_L on D and α complicates correcting k_L values determined using a reference tracer gas to a second species of interest (Asher and Wanninkhof, 1997). This is especially true when the reference tracer and the gas of interest have very different solubilities.

Bubble-mediated transfer further complicates the use of reference tracer species by causing k_L measured for invasion to be larger than k_L measured for evasion. Memery and Merlivat (1985) showed that this asymmetry increases as the system nears equilibrium (i.e., as ΔC approaches zero) or as α decreases. Most of the purposeful reference tracers used in gas exchange studies have small α, very large ΔC, and typically measure k_L for evasion only. However, it is important to know both the invasion and evasion rates of environmentally important gases. Furthermore, the gas of interest could have a very different solubility from the tracer and may have a concentration difference that is close to equilibrium. This makes it difficult to estimate its k_L based on the k_L value measured only for evasion of the reference gas.

As a preliminary step in developing a general relation for estimating oceanic k_L values at all values of ΔC for both invasion and evasion, Asher *et al.* (1996) parameterized bubble-mediated transfer in seawater when the air-water concentration difference was far from equilibrium. In particular, when $\Delta C \gg 0$ (i.e., invasion) or $\Delta C \ll 0$ (i.e., evasion) they showed that k_L could be partitioned using the fractional area bubble plume coverage, B_C, as

$$k_L = (k_M + B_C(k_T - k_M)) + B_C k_B \tag{2}$$

where k_M is the transfer velocity due to turbulence generated by a mixing pump, k_T is the transfer velocity due to turbulence generated by the simulated breaking wave, and k_B is the bubble-mediated transfer velocity. As defined in (2), k_B is the transfer velocity of the entire bubble plume and is a function of the number size spectra of all of the bubbles in the plume. It should not be confused with the transfer velocity of an individual bubble. Asher *et al.* (1996) showed that k_B could be parameterized as

$$k_B = \frac{a_1}{\alpha} + b_1 \alpha^{-m} Sc^{-n'} \tag{3}$$

where a_1, b_1, m, and n' are constants determined separately for evasion and invasion in seawater by measuring k_L for carbon dioxide (CO_2), dimethyl sulfide (DMS), helium (He), oxygen (O_2), and sulfur hexafluoride (SF_6). However, Asher *et al.* (1995) found that the seawater coefficients were not applicable to freshwater, suggesting that there were differences in the bubble-mediated transfer process between the two media.

In (2), both k_M and k_T can be expanded using (1) with a proportionality constant, A, that is determined by the mechanically generated and plume-related turbulence, respectively. By substituting the form for k_B given in (3) and expanding k_M and k_T, (2) can be written

$$k_L = [A_M + B_C(A_T - A_M)]Sc^{-n} + B_C\left(\frac{a_1}{\alpha} + b_1\alpha^{-m}Sc^{-n'}\right) \tag{4}$$

where A_M and A_T are the proportionality constants for k_M and k_T, respectively, and a_1, b_1, m, and n' are the constants defined in (3). The portion of k_L that is due to turbulence-mediated processes, Φ_T, and the portion that is due to bubble-mediated processes, Φ_B, are defined by

$$\Phi_T = [A_M + B_C(A_T - A_M)]Sc^{-n} \tag{5}$$

and

$$\Phi_B = B_C\left(\frac{a_1}{\alpha} + b_1\alpha^{-m}Sc^{-n'}\right) \tag{6}$$

which are the first and second terms, respectively, on the right-hand side of (4).

A detailed study was conducted to examine the behavior of bubble populations and Φ_B in freshwater and seawater. Identifying the causes for the differences in Φ_B between the two media will help in determining the possible errors associated with applying results from measurements made in freshwater systems to transfer in seawater. Understanding the role that changes in the bubble population have in affecting the behavior of Φ_B will help both in determining the limitations associated with applying laboratory measurements to oceanic conditions and in developing a parameterization of oceanic gas transfer velocities in the presence of breaking waves applicable to both evasion and invasion.

2. Experimental techniques

The measurements discussed here were made in a whitecap simulation tank (WST). The WST was a 1.2-m by 1.2-m by 1.8-m acrylic tank with a water depth of 1.2 m and a water volume of 1.7 m³. It had a computer-controlled tipping bucket that generated reproducible, simulated breaking waves by releasing 0.02 m³ of water vertically onto the tank water surface. Water temperature, T_W, was regulated with a precision of 0.5 K using a flow-through chiller-heater and the aqueous phase was continuously homogenized using a small submersible pump. T_W and air temperature were measured using NBS-traceable mercury thermometers or platinum resistance thermistors. The details of the tank and its operation are described by Asher and Farley (1995) and Asher *et al.* (1996).

The instantaneous fraction of the water surface covered by the active bubble plume, $\phi(t_A)$, at time, t_A, after generation of the plume was calibrated in the WST for freshwater and seawater using a video procedure similar to that described by Monahan (1989). First, the grey-scale brightness value of a patch of surface containing an actively entraining bubble plume was determined by manual inspection of a digitized video frame. The

Table 1. Bucket parameters in freshwater and seawater.

		B_C	
V_F, m^3	t_B, s	FW	SW
0.020	30	0.0038	0.0077
0.020	36	0.0031	0.0064
0.020	55	0.0021	0.0042
0.020	110	0.0010	0.0021
0.0	∞	0.00	0.00

fraction of the image in a frame that was above this threshold gave an estimate of $\phi(t_A)$. A time series of $\phi(t_A)$ over the lifetime of the plume was generated by analysis of every third video frame. The lifetime of an individual plume in its active stage, t_P, was defined as the time interval over which $\phi(t_A)$ first increased above and then returned to zero. The time-averaged fractional area bubble plume coverage, B_C, was calculated from $\phi(t_A)$ by

$$B_C = \frac{1}{t_B} \int_0^{t_P} \phi(t_A) \, dt_A \tag{7}$$

where t_B is the time between successive bubble plumes. Table 1 lists t_B, B_C, and bucket fill volume, V_F, used for freshwater and seawater. In freshwater, $t_P = 2.2$ s and $t_P = 5.7$ s in seawater. The differences in B_C at the same t_B between freshwater and seawater are discussed in Section 3a.

The grey-scale analysis used here provided an estimate of the area of the water surface covered by a bubble plume that had an albedo of greater than approximately 0.5. This albedo was observed in plumes that were actively entraining air or in the early stages of decay. Using this definition, B_C is analogous to the "Stage A" whitecap coverage defined by Monahan (1989). Furthermore, the analysis in Section 3a showed that the time required for most of the bubbles generated by the breaking event to return to the surface (i.e., the total lifetime of the bubble plume) was considerable longer than t_P. Following the analogy with Stage A whitecaps, t_P will be referred to as the lifetime of the Stage A (or active) bubble plume.

The freshwater measurements were made using tapwater that was drawn from a 150-m deep on-site well and then filtered through a 5-μm spun-fiber filter and sterilized using a flow-through ultraviolet (UV) water sterilizer. Contaminants on the water surface were removed by vacuuming the surface prior to the start of each experiment. Water prepared in this manner will be referred to as "cleaned." For comparison with the cleaned experiments, water that was known to be affected by the presence of surfactants was generated by adding 1.9×10^{-3} kg of Triton X-100. This resulted in a surfactant concentration of 1.1×10^{-3} kg m^{-3}. Experiments in water containing Triton X-100 are termed surfactant-influenced (SI).

The freshwater gas transfer experiments were conducted at $T_W = 293$ K. Transfer velocities in cleaned freshwater were measured as a function of B_C for evasion of CO_2, He, O_2, and SF_6 and invasion of O_2. Transfer velocities in SI freshwater were measured for

Table 2. Schmidt numbers and Ostwald solubilities in freshwater and seawater.

		Schmidt Number		Ostwald Solubility	
Gas	T_W, K	Sc(FW)	Sc(SW)	α(FW)	α(SW)
CO_2	293	600†	666†	0.94*	0.87*
He	293	149†	165†	0.0094†	0.0082†
O_2	293	530†	589†	0.033†	0.028†
SF_6	293	958†	1066†	0.0066†	0.0047†

†Wanninkhof (1992)
*DOE (1994)

evasion of CO_2, He, and SF_6 and invasion of O_2. Sc and α in freshwater and seawater at $T_W = 293$ K for He, SF_6, CO_2, and O_2 are listed in Table 2. The seawater gas transfer data used here were measured by Asher et al. (1996).

The experimental protocols and analytical techniques used for measuring aqueous-phase concentrations of CO_2, He, O_2, and SF_6 have been explained in detail by Asher et al. (1996) and were used here without modification. Briefly, He and SF_6 were analyzed by gas chromatography using the syringe-headspace method developed by Wanninkhof et al. (1991). Both the partial pressure of CO_2 in the air and the aqueous-phase partial pressure of CO_2, pCO_2, were measured chromatographically. The freshwater CO_2 experiments were conducted by acidifying the water in the WST using hydrochloric acid so that the change in total CO_2 concentration could be tracked by measuring the decrease in pCO_2. Evasion rates of CO_2, He, and O_2 were measured by adding each gas to the water by bubbling pure gas into the tank through gas permeable tubing. Evasion of SF_6 was studied by adding a concentrated aqueous-phase solution of the gas to the tank. Invasion rates for O_2 were measured by sparging O_2 from the water using He as the stripping gas. Further details concerning the experimental procedures and data reduction techniques have been provided by Asher et al. (1996).

Bubble size and velocity in the freshwater and seawater plumes were measured with a phase-Doppler anemometer (PDA). Asher and Farley (1995) have shown that the PDA provided accurate measurements of bubble concentrations and velocities in the WST and their PDA configuration was used here. The minimum and maximum bubble radius, r, that could be measured in the WST were 50 μm and 1100 μm, respectively, with a radius resolution of 5.5 μm. The minimum and maximum velocities that could be measured were -1.46 m s^{-1} and 0.49 m s^{-1} (positive velocities were directed toward the water surface) with a resolution of 0.01 m s^{-1}. PDA measurements were made as a function of depth in the center of the plume. Each PDA data set consisted of a time series of bubble radii and velocities collected over at least 60 sequential simulated breaking waves. For $t_B = 30$ s, these time series were 1800 s long and contained data for 1000 to 4000 bubbles depending on water type and measurement depth.

The time index in each PDA data record was given by the sampling time of the bubble in the total data record. Because a single plume did not provide a high enough bubble density over the plume lifetime to allow detailed study, it was necessary to combine the data for at

least 60 sequentially generated bubble plumes. The computer controlling the tipping bucket generated an electronic event marker at the start of each simulated breaking wave that was encoded by the PDA processing electronics. Therefore, each bubble measured by the PDA also was tagged with the arrival time after the generation of the most recent plume, t_A. Analysis of the temporal spacing of these event markers and subsequent generation of bubbles showed that the uncertainty in determining the starting time for each plume in the record was 20 ms ($\pm 1\sigma$). Because the bucket mechanism in the WST functioned so consistently, bubbles measured over 60 sequential plumes could be combined into one time series using t_A as the time index rather than the sample time relative to the start of the data record.

Bubble velocities, v_z, at a depth of 0.25 m were studied using the aggregate PDA data records described above. Spectral analysis found that the dominant wave motions had frequencies centered at 1.4 Hz. These motions were removed by digital filtering using a fifth-order band-stop Chebyshev filter at a center frequency of 1.4 Hz with a bandwidth of 0.3 Hz. The overall behavior of v_z in the plume was observed by low-pass filtering the resulting time series at a frequency of 3 Hz. Representative samples for the raw aggregate time series, the time series resulting from the band-stop digital filter, and the results from low-pass filter are shown below.

The ascending plume typically lasted from $t_A \approx 1.5$ s until $t_A \approx 10$ s. Average bubble rise velocities, v_B, in the ascending plume were estimated by sorting all bubbles into their respective size classes. Then, the individual velocities of all bubbles with a particular radius were averaged together. Because some size classes contained only a few bubbles, the data were badly scattered and not easily visualized. Therefore, the rise velocities over 5 adjacent radii were also averaged. This significantly reduced the scatter and the results are shown below.

Bubble populations at a depth of 0.15 m in the center of the bubble plume were measured using the PDA. Five separate 1800-s long data records each for cleaned seawater and cleaned freshwater were available. Four separate 1800-s records were available for SI seawater, and there were two records for SI freshwater. Bubble concentrations, $n(r)$ (number of bubbles per cubic meter per unit increment of radius), averaged over the multiple records and their associated standard deviations were calculated using the procedure described by Asher and Farley (1995). This method produced bubble concentrations that were time-averaged over t_B, which was 30 s for these data. The $n(r)$ were normalized to $B_C = 0.0038$ as described by Asher and Farley (1995). Since B_C was already equal to 0.0038 for $t_B = 30$ s in freshwater, this normalization was only applied to the seawater data sets. Operationally, $n(r)$ in cleaned and SI seawater was normalized to $B_C = 0.0038$ by dividing the concentrations measured for $t_B = 30$ s by a factor of two.

3. Results and discussion

a. Bubble population, water velocity, and bubble plume coverage measurements. Figure 1 shows time series of vertical bubble velocities, v_z, plotted versus t_A for cleaned freshwater, SI freshwater, cleaned seawater and SI seawater. For $t_A > 5$ s, the vertical motions caused
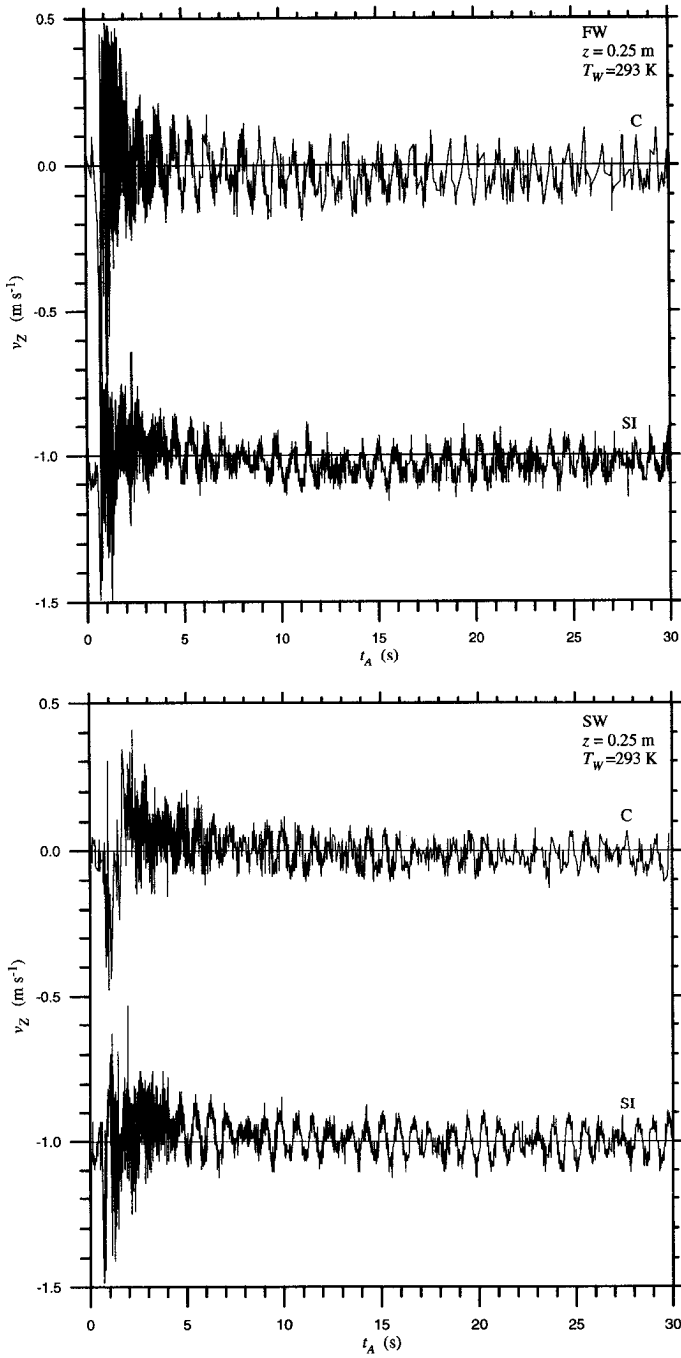
Figure 1.

by waves generated during the creation of the bubble plume are evident. The reproducibility of the bubble plumes is demonstrated by presence of these wave motions in each combined data set. If the 60 different whitecaps used to generate each time series in Figure 1 were being generated at different times, their random phase lags would cause the wave motions to appear as uncorrelated noise. Spectral analysis has shown that the oscillations with a frequency of approximately 0.1 Hz visible in the data were actually the beat frequency of two separate wave modes in the WST, one at 1.35 Hz and one at 1.45 Hz.

Because each of the four time series in Figure 1 was generated by combining data from 60 different plumes, the velocities of sequential points were not necessarily correlated at small scales. This and the absence of a mean flow necessary for applying Taylor's hypothesis precluded extracting the turbulence length and velocity scales from the data. However, it is possible to gain some information concerning the vertical water motions by examining the digitally filtered velocity records shown in Figure 2. With the large-scale wave motions removed, each of the time series shows the initial downward plunging mass of water entraining bubbles ($v_z < 0$) from $t_A = 0.5$ s until $t_A = 1.5$ s and the subsequent rise of bubbles ($v_z > 0$) back to the surface from $t_A = 1.5$ s onward.

For the data in Figure 2 with $t_A > 10$ s, the RMS value for the fluctuations in v_z in cleaned freshwater was 0.036 m s^{-1} and the corresponding RMS value for v_z in cleaned seawater was 0.030 m s^{-1}. Although these cannot be directly related to turbulence velocity scales, it does indicate that the small-scale fluctuations were 20% larger in cleaned freshwater than in cleaned seawater. The vertical velocities due to waves decay exponentially with depth on a scale related to wavelength and the digital filter removed motions associated with the largest waves. Therefore, it is likely that at $z = 0.25$ m turbulence was a significant source of velocity fluctuations. The RMS values for SI freshwater and SI seawater were 0.029 m s^{-1} and 0.021 m s^{-1}, respectively, suggesting that the surfactant decreased turbulence velocities in both media.

The behavior of v_z can be more clearly seen in Figure 3, which shows the result of low-pass filtering each of the time series in Figure 2. Once the upward moving bubble plume had risen through the sample volume, the average velocity returned to zero. The time it took for this to occur provided an estimate of the total plume lifetime. However, the total plume lifetime was longer than t_P, the lifetime of the Stage A plume. This occurred because the albedo of a plume of decaying bubbles was below the brightness threshold used in the video analysis of B_C.

The average value of v_z returned to zero after approximately 9 s in both cleaned and SI seawater. The data for cleaned freshwater in Figure 3 show that the time when v_z returns to zero was somewhat indeterminate although it most likely was between 7 s and 9 s. In

---

Figure 1. Plot of the vertical bubble velocities, v_z, as a function of time after creation of the plume, t_A. The measurements were made at a depth, z, of 0.25 m in the center of the plume and at a water temperature, T_W, of 293 K. (a) v_z measured in cleaned (C) and surfactant-influenced (SI) freshwater (FW) and (b) v_z in C and SI seawater (SW). For clarity, v_z(SI) has been offset from v_z(C) by subtracting 1.0 m s^{-1} from each point in the time series.
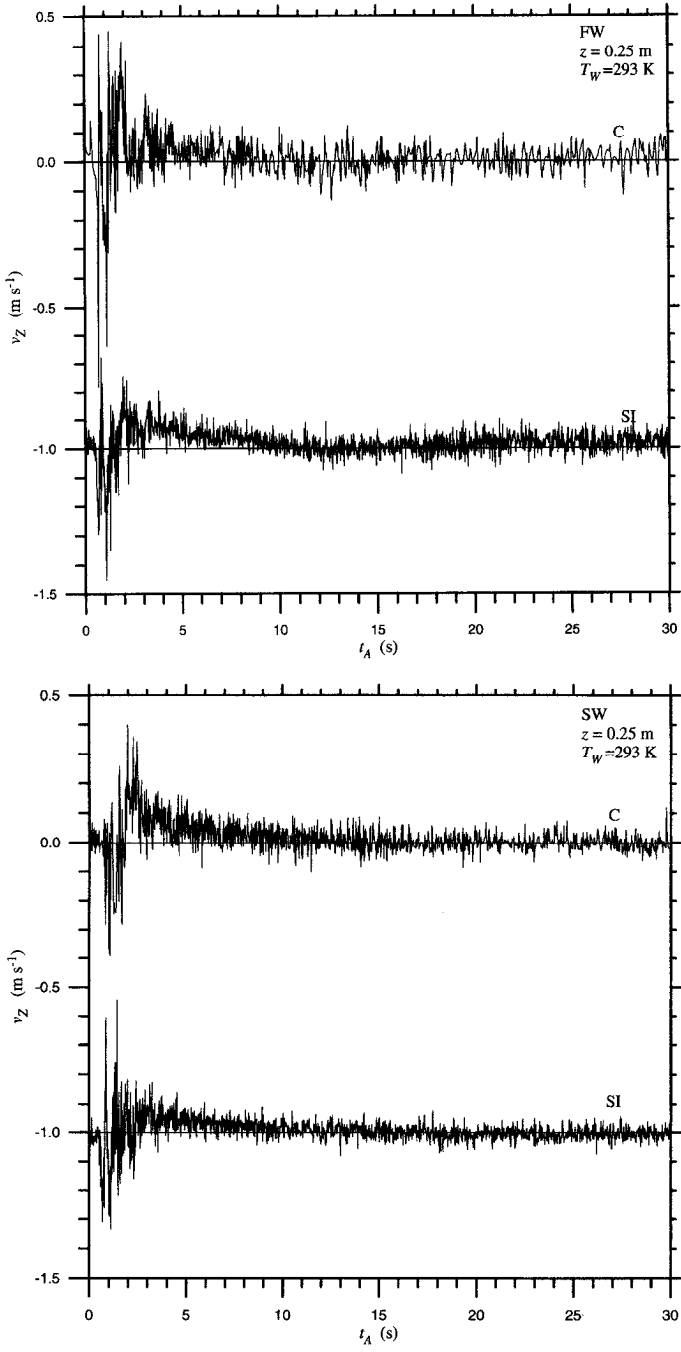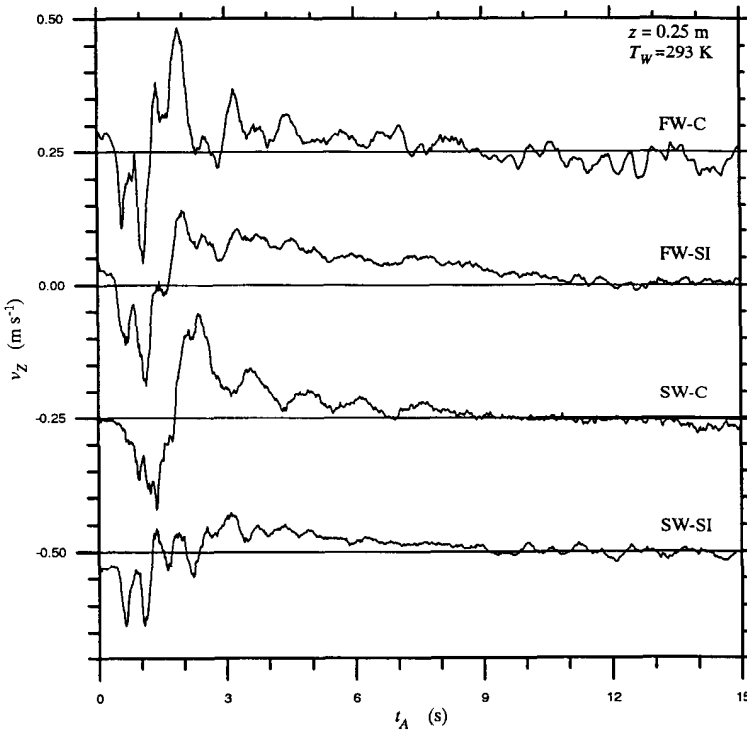
Figure 2.

Figure 3. Plot of the result of passing each of the time series for the vertical bubble velocity, v_z, shown in Figure 2 through a 3-Hz low-pass digital filter. Data are shown for cleaned (C) and surfactant-influenced (SI) seawater (SW) and for C and SI freshwater (FW). For clarity, the FW-C time series has been offset by adding 0.25 m s^{-1} to each point in the series, the SW-C series has had 0.25 m s^{-1} subtracted from each point, and the SW-SI series has had 0.50 m s^{-1} subtracted from each point. The measurements were made at a depth, z, of 0.25 m and at a water temperature, T_W, of 293 K.

contrast to cleaned freshwater, v_z in SI freshwater returned to zero after 12 s. In both freshwater and seawater, the addition of the surfactant decreased the maximum observed upward bubble velocity. This decrease was most likely caused by the surfactant reducing the rise velocities of the bubbles in the plume (Clift *et al.,* 1978).

Figure 4 shows $n(r)$ calculated from the PDA data. As was observed by Asher and Farley (1995), there was little difference between $n(r)$ for cleaned and SI seawater. There were more larger bubbles ($r > 500$ µm) generated in the cleaned freshwater plumes than in the

Figure 2. Plot of the digitally filtered vertical bubble velocities, v_z, as a function of time after the creation of the plume, t_A. The measurements were made at a depth, z, of 0.25 m in the center of the plume and at a water temperature, T_W, of 293 K. (a) v_z measured in cleaned (C) and surfactant-influenced (SI) freshwater (FW) and (b) v_z in C and SI seawater (SW). For clarity, v_z(SI) has been offset from v_z(C) by subtracting 1.0 m s^{-1} from each point in the time series.
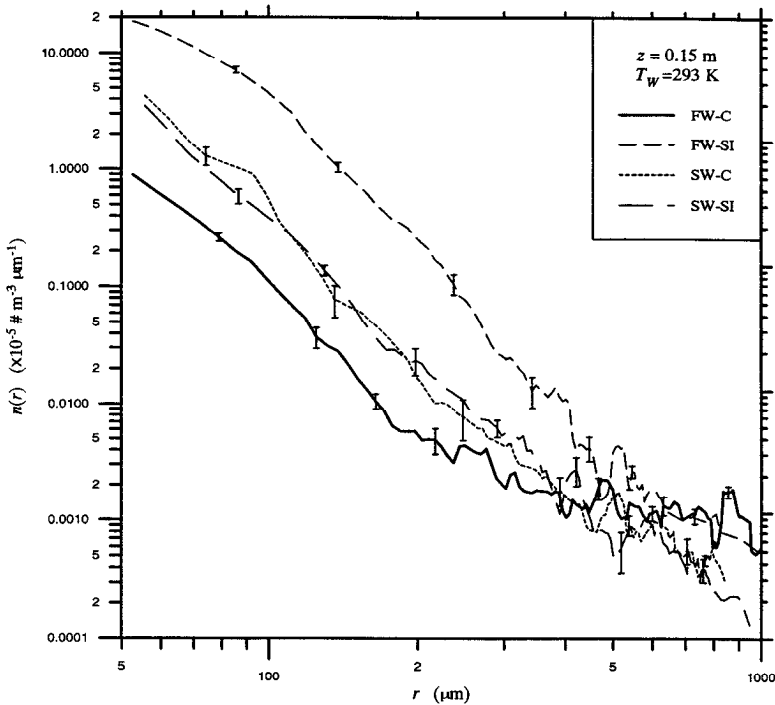
Figure 4. Size-segregated bubble concentrations, $n(r)$, plotted versus radius, r, as measured in the whitecap simulation tank using the phase-Doppler anemometer. All data were collected at a depth, z, of 0.15 m and at a water temperature, T_W, of 293 K for cleaned (C) and surfactant-influenced (SI) freshwater (FW) and seawater (SW) bubble plumes. The $n(r)$ shown are the average values of multiple independent data records (5 each for FW-C and SW-C, 4 for SW-SI and 2 for FW-SI). The data key is shown on the figure. The error bars represent the standard deviation of the mean value ($\pm 1\sigma$) for FW-C, SW-C, and SW-SI. The error bars for FW-SI show the range of $n(r)$.

cleaned seawater plumes. This agrees with the results of Shatkay and Ronen (1992), Haines and Johnson (1995) and Wanninkhof *et al.* (1995), who also observed that the concentration of large bubbles was higher in freshwater than in seawater. Figure 4 also shows that for $r < 300$ μm, $n(r)$ was larger in cleaned seawater than $n(r)$ in cleaned freshwater.

The presence of the surfactant in freshwater had a large effect on bubble populations. In fact, the increase in the concentration of small bubbles for SI freshwater was so large that it was obvious to the naked eye. The PDA data showed that for $r < 500$ μm, $n(r)$ for SI freshwater was over an order of magnitude larger than $n(r)$ for cleaned freshwater. The exact reasons why Triton X-100 had such a large effect on the bubble populations in freshwater but such a small effect in seawater are not definitively known at present. It is known that the presence of electrolytes increases the film pressure of a nonionic soluble surfactant such as Triton X-100 and causes the surfactant to behave more like an insoluble
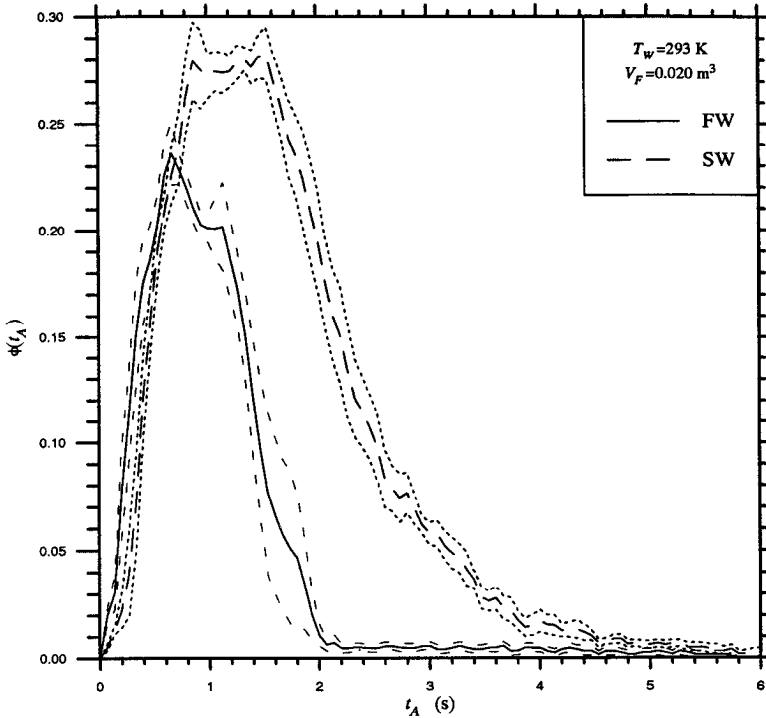
Figure 5. The instantaneous bubble plume coverage, $\phi(t_A)$, plotted versus time after the creation of the plume, t_A, for cleaned freshwater (FW) and cleaned seawater (SW). The data are mean values of $\phi(t_A)$ computed from 12 separate plumes generated at a water temperature, T_W, of 293 K using a bucket volume, V_F, of 0.020 m^3. The heavy solid line is the average $\phi(t_A)$ calculated for the freshwater bubble plumes. The light dashed lines show the envelope of the standard deviation ($\pm 1\sigma$) of the average freshwater $\phi(t_A)$. The heavy dashed line and light dotted lines show the equivalent information for the seawater bubble plumes.

surfactant [Hsiao *et al.,* 1956; Lange and Jeschke, 1987]. However, the exact mechanisms by which this effect leads to the difference in bubble populations remain speculative.

The data in Table 1 show that at the same t_B, the seawater B_C values were nearly a factor of two larger than B_C in freshwater; a result consistent with the previous measurements made by Monahan and Zietlow (1969). Figure 5 shows $\phi(t_A)$ averaged over 12 separate freshwater and seawater bubble plumes. The data show that $t_P = 2.2$ s in freshwater and that $t_P = 5.7$ s in seawater (t_P in Figure 5 is equal to the time required for $\phi(t_A)$ to rise above and return to its initial value). Furthermore, the maximum value of $\phi(t_A)$ in seawater was 0.28 and the maximum value of $\phi(t_A)$ in freshwater was 0.24. The increase in both t_P and the maximum of $\phi(t_A)$ for seawater explain why B_C calculated using (7) for constant t_B was larger in seawater than freshwater.

The explanation for why t_P and the maximum value of $\phi(t_A)$ increased from freshwater to seawater lies in the interaction between the bubble residence times and $n(r)$ in the two
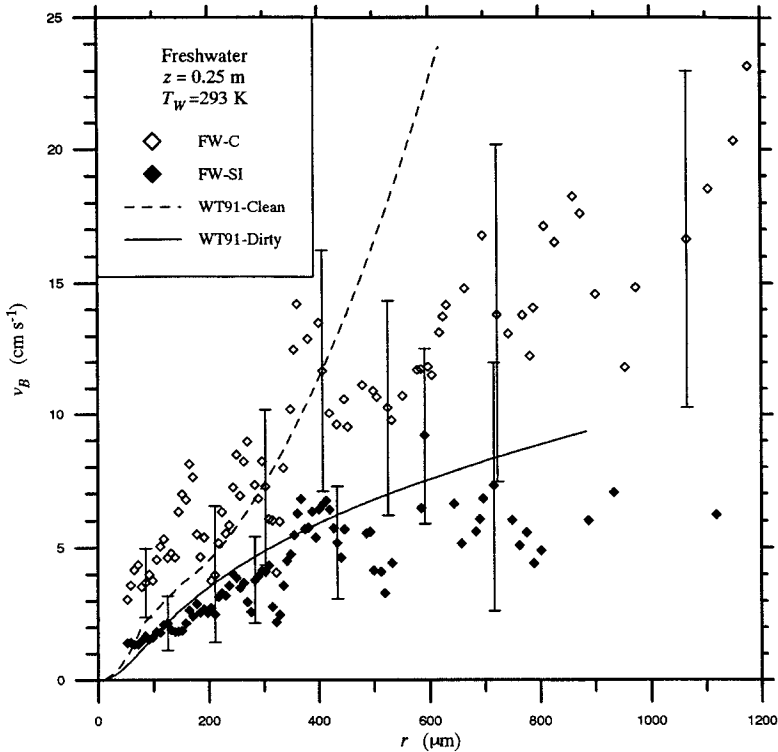
Figure 6. Average bubble rise velocity, v_B, plotted as a function of bubble radius, r, for bubble populations measured at a depth, z, of 0.25 m and at a water temperature, T_W, of 293 K. v_B measured in cleaned (C) and surfactant-influenced (SI) freshwater and (b) v_B measured in C and SI seawater. Also shown are bubble rise velocities calculated for clean and dirty bubbles using the relations from Woolf and Thorpe (1991) [WT91]. The data key is shown on the figure.

plumes. Figure 6 shows v_B calculated from the PDA data in Figure 2 for the time interval 1.5 s $< t_A <$ 6 s. Comparing v_B between cleaned freshwater and cleaned seawater showed that v_B was essentially equal for bubbles with $r <$ 300 μm but that v_B was significantly higher in freshwater than in seawater for $r >$ 300 μm. This implies that the residence times of large bubbles in cleaned freshwater were smaller than the residence times of large bubbles in seawater. Furthermore, there were fewer small bubbles with longer residence times in cleaned freshwater compared to cleaned seawater (note that this was true even for bubble populations that had not been normalized to a common B_C). The albedo of a plume was related to the total number of bubbles in the plume, and it was the albedo that controlled $\phi(t_A)$, t_P, and B_C. Therefore, the combination of fewer smaller bubbles and the shorter lifetime of the larger bubbles resulted in a shorter t_P and a lower total albedo in freshwater, which resulted in smaller $\phi(t_A)$ (and B_C) in freshwater.

Figure 6 also shows that addition of the surfactant to freshwater had a large effect on v_B for all bubble sizes. This reduction in rise velocity would have caused an increase in the
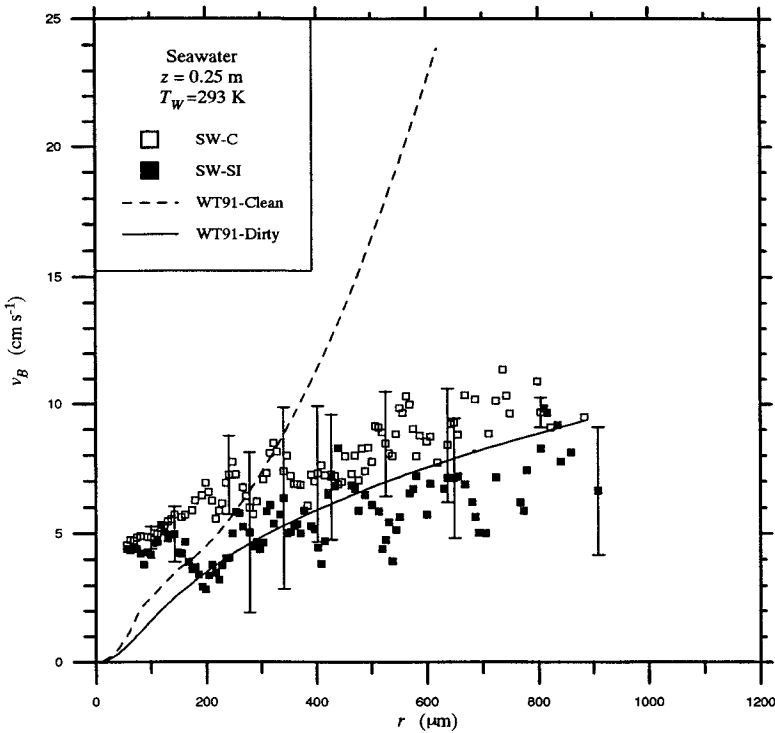
Figure 6. (Continued)

total plume lifetime, as was seen in the data in Figure 3. In seawater, the surfactant reduced v_B slightly for bubbles with $r > 200$ μm. The similarity in v_B for the smaller bubbles in seawater explains why the surfactant had little effect on the total plume lifetime in seawater (see Fig. 3).

The presence of the surfactant led to stable foam patches on the water surface in the WST when bubble plumes were generated. These foam patches prevented the calibration of B_C for SI waters. Therefore, it was assumed that B_C was equal for cleaned and SI water. The similarity in $n(r)$ and v_B between cleaned seawater and SI seawater (see Figs. 4 and 6b) provides strong evidence that this was a reasonable assumption for seawater. However, based on the freshwater bubble data in Figure 4 and the velocity data in Figure 6a it is likely that B_C at a given t_B was higher in SI freshwater than in cleaned freshwater. However, it is not possible to quantify this difference using the current data set and it is unlikely that further measurements will be made in the WST. The possible impact of underestimating B_C for SI freshwater on the gas exchange results will be discussed where appropriate in the following analysis.

In the preceding analyses, if B_C in SI freshwater has been underestimated by a factor of two, the bubble concentrations shown in Figure 4 should be a factor of two smaller. In this case the concentration of small bubbles in SI freshwater would still be larger than in all the
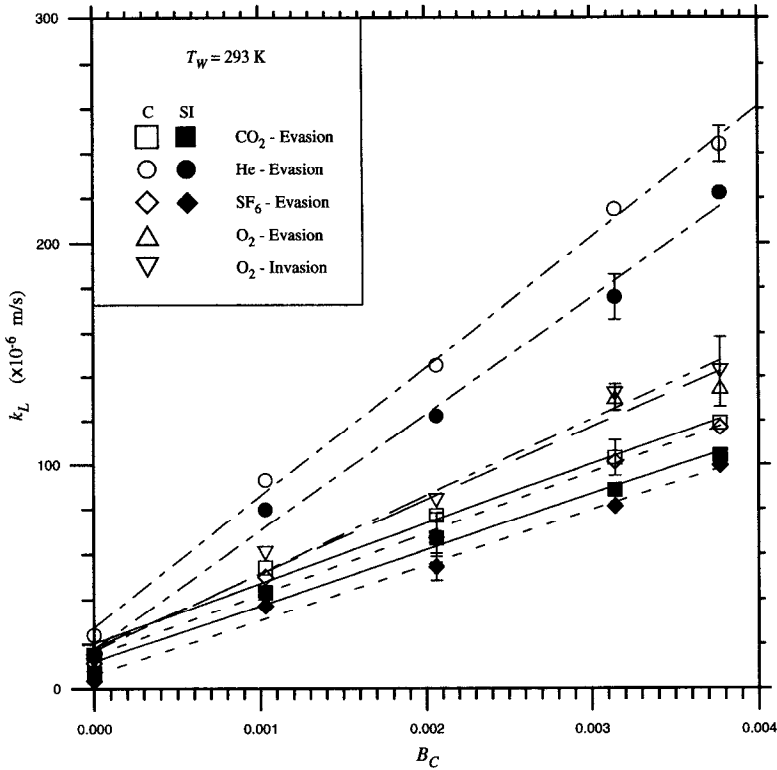
Figure 7. The gas transfer velocity, k_L, measured in cleaned (C) freshwater for evasion of CO_2, He, O_2, and SF_6 and for invasion of O_2 plotted versus bubble plume coverage, B_C. Also shown is k_L measured for evasion of CO_2, He, and SF_6 and invasion of O_2 in surfactant-influenced (SI) water. All data were measured at a water temperature, T_W, of 293 K. The straight lines are plots of a linear regression of each data set. The error bars show the experimental uncertainty ($\pm 1\sigma$). The data key is shown on the figure.

other media, but the concentration of large bubbles in SI freshwater would be lower than the concentrations in cleaned freshwater but higher than the seawater concentrations. The analysis concerning v_B would be unchanged by underestimation of B_C.

b. Gas transfer measurements. Figure 7 shows k_L for evasion of CO_2, He, O_2, and SF_6 and k_L for invasion of O_2 in cleaned freshwater plotted versus B_C. Figure 7 also shows k_L for evasion of CO_2, He, and SF_6 in SI freshwater. All of the data were measured at $T_W = 293$ K. The result from a linear regression of k_L versus B_C for each data set is shown on the figure and in Table 3. As was observed by Asher *et al.* (1996) for seawater, the freshwater k_L values were linearly correlated with B_C.

If the bubble-mediated gas flux was negligible, k_L for the different gases should have been proportional to Sc^{-n}. For $n = \frac{1}{2}$, k_L for SF_6, $k_L(SF_6)$, should have been 26% smaller than k_L for CO_2, $k_L(CO_2)$, given that Sc for SF_6 is 60% larger than Sc for CO_2 (see Table 2). Because the typical experimental uncertainty in measuring k_L in the WST was $\pm 10\%$, this

Table 3. Results of linear regression of k_L versus B_C: k_L = slope $\times$ B_C + intercept.

Gas	Slope Value	$\pm 1\sigma$	Intercept Value	$\pm 1\sigma$	r^2	σ	d.f.†
k_L ($\times 10^6$ m s^{-1}), evasion, cleaned freshwater							
CO_2	26600	1600	20	5	0.989	5	3
He	58300	1600	28	5	0.998	5	3
O_2	33000	4200	18	13	0.985	11	1
SF_6	27200	1600	15	5	0.989	5	3
k_L ($\times 10^6$ m s^{-1}), invasion, cleaned freshwater							
O_2	34600	2400	17	7	0.985	8	3
k_L ($\times 10^6$ m s^{-1}), evasion, SI freshwater							
CO_2	24900	1600	12	5	0.987	5	3
He	52600	2500	18	8	0.993	8	3
SF_6	24500	1400	6	4	0.991	4	3
k_L ($\times 10^6$ m s^{-1}), invasion, SI freshwater							
O_2	28500	500	7	2	0.999	2	3

†d.f. is degrees of freedom.

difference should be observable in the data. In support of this, for B_C = 0.00 the data in Figure 7 show that $k_L(CO_2)$ was 35% larger than $k_L(SF_6)$ (i.e., the measured and expected differences were within the limits of the experimental uncertainties). However, when B_C = 0.0038 the data show that $k_L(SF_6)$ was only 2% smaller than $k_L(CO_2)$, or the observed difference between the measure values was significantly smaller than the predicted difference. This implies that some exchange process preferentially increased the transfer velocity of SF_6 over the transfer velocity of CO_2 when bubbles were present. Furthermore, assuming that $\frac{1}{2} \leq n \leq \frac{2}{3}$ shows that this process cannot be parameterized using a function of the form given in (1).

That this preferential increase in $k_L(SF_6)$ was caused by bubble-mediated transfer can be seen by calculating the ratio in the slopes resulting from the linear regression of k_L with respect to B_C for the different gases. If the increases in k_L were due solely to turbulence then the slopes for different gases should have been related through their Sc values and (1). However, models (Memery and Merlivat, 1985; Woolf and Thorpe, 1991) and experiments (Asher et al., 1996) have shown that k_B is a function of Sc and α, with k_B increasing as α decreases at constant Sc. Therefore, if a significant fraction of the total measured k_L was due to bubble mediated processes, changes in α between different gas pairs will cause the measured ratio in slope to be different from that predicted using (1). For example, α for SF_6 is two orders of magnitude less than α for CO_2 but their Sc values differ by only 60% and bubble-mediated processes should cause a larger increase in $k_L(SF_6)$ than $k_L(CO_2)$ at a given B_C.

Using $n = \frac{1}{2}$ in (1) shows that the ratio of the slope for CO_2 to the slope for SF_6 should

be 1.26 (note that assuming $n > \frac{1}{2}$ further increases the ratio of the two slopes). The regression results in Table 3 show that in freshwater the ratio of the slope for CO_2 to the slope for SF_6 was 0.98, which is significantly less than the predicted ratio. This implies that the slope for SF_6 was larger than expected based on turbulence-driven exchange and, as stated above, consistent with the hypothesis that bubble-mediated processes were responsible for a significant fraction of the increase in k_L. In fact, comparing the predicted and observed ratios in the slopes of other gas pairs showed that k_L for $B_C > 0.00$ could not be parameterized as shown in (1) and that the difference between the ratios was consistent with that predicted by bubble-mediated exchange models. This suggests that bubble-mediated processes were responsible for a significant fraction of the increase in k_L with increasing B_C.

In agreement with the data of Asher *et al.* (1996) for gas transfer in seawater, comparing the data for cleaned freshwater to the data for SI freshwater showed that the presence of the surfactant decreased k_L for each gas at all B_C. Comparing the ratio of the measured slopes of the linear regressions for a particular pair of gases to the ratio of the slopes predicted assuming that k_L was proportional to $Sc^{-2/3}$ showed that bubble-mediated processes were also important in SI freshwater. Neither of these conclusions would be affected by underestimation of B_C in SI freshwater. However, underestimation of B_C in SI freshwater would increase the difference between k_L measured for cleaned freshwater and k_L measured for SI freshwater.

Figure 8 is a comparison of cleaned freshwater and cleaned seawater k_L values for evasion of CO_2, He, and SF_6. The seawater k_L values are from Asher *et al.* (1996). For equivalent B_C in both media, k_L in freshwater was larger than k_L in seawater for all three gases. This is not particularly surprising because the modeling studies of Keeling (1993) and Woolf (1993) have shown that large bubbles can transfer more gas than small bubbles. The increased effectiveness of freshwater plumes relative to seawater plumes at a given value of B_C results from the increased concentration of larger bubbles in freshwater plumes.

4. Bubble-mediated gas transfer

Comparison of the turbulence and bubble-mediated transfer fractions in freshwater and seawater requires determining the coefficients for Φ_T and Φ_B defined in (5) and (6), respectively, for each media. Asher *et al.* (1996) found A_M and n for cleaned and SI seawater by linear regression of $\ln(k_L)$ versus $\ln(Sc)$ for k_L measured when $B_C = 0.00$ and calculated A_T, a_1, b_1, m, and n' for cleaned and SI seawater by nonlinear optimization of experimental data measured for $B_C > 0.00$ to (4) using the A_M and n determined for the $B_C = 0.00$ data. The fitting parameter, χ^2, for the optimization used by Asher *et al.* (1996) was

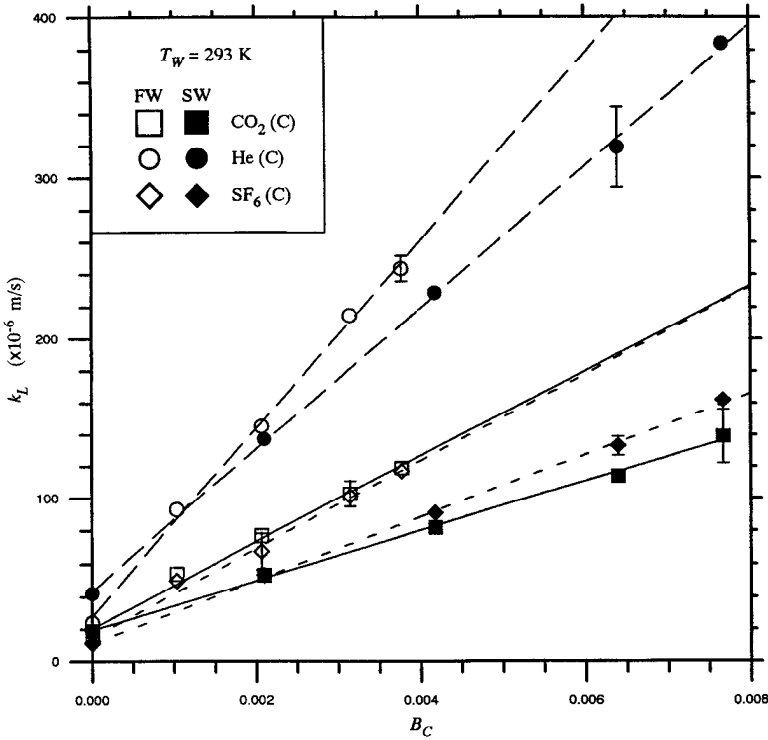$$\chi^2 = \sum_{i=1}^{j} \frac{[k_{L,i} - (\Phi_T(i) + \Phi_B(i))]^2}{\sigma_i^2} \tag{8}$$

Figure 8. The gas transfer velocity, k_L, for evasion of CO_2, He, and SF_6 through cleaned (C) freshwater (FW) and seawater (SW) plotted versus bubble plume coverage, B_C, at a water temperature, T_W, of 293 K. The SW data is from Asher *et al.* (1996). The straight lines are plots of a linear regression of each data set. The error bars show the typical experimental uncertainty ($\pm 1\sigma$). The data key is shown on the figure.

where the summation was over all gases measured at $B_C = 0.0077$ and σ_i^2 was the experimental variance of $k_{L,i}$. Here, A_M and n for cleaned and SI freshwater were determined as described by Asher *et al.* (1996) using the data for $B_C = 0.00$. However, because fewer measurements were available at each B_C, the summation in (8) used to calculate the coefficients for Φ_B ran over all gases measured for $B_C > 0.00$.

Table 4 shows n, A_M, A_T, a_1, b_1, m, and n' determined for evasion in cleaned and SI freshwater and the n, A_M, A_T, a_1, b_1, m, and n' calculated by Asher *et al.* (1996) for evasion in cleaned and SI seawater. Figure 9 shows the normalized difference, E_N, between k_L predicted using (4) and the freshwater coefficients listed in Table 4 and k_L measured in the WST plotted versus B_C for evasion in both cleaned freshwater and in SI freshwater. Following the notation used by Asher *et al.* (1996), E_N is given by

$$E_N = 100 \left| \frac{k_L(\text{Predicted})}{k_L(\text{Measured})} - 1 \right| \tag{9}$$

Table 4. Optimization results for evasion in freshwater and seawater.

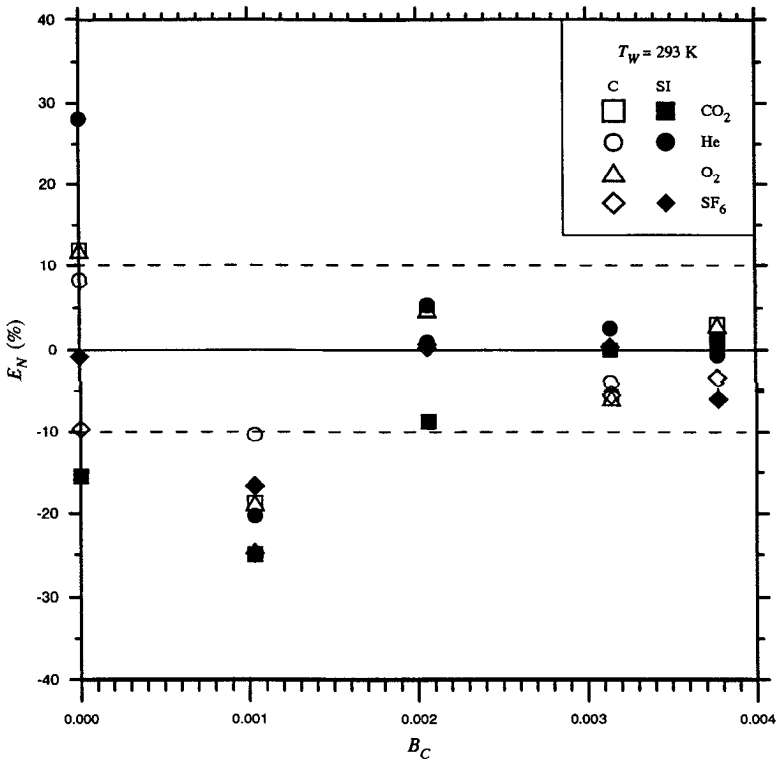|	Freshwater		Seawater	
	Cleaned	Surfactant-influenced	Cleaned	Surfactant-influenced
n	0.50	0.67	0.56	0.63
A_M, m s^{-1}	3.0×10^{-4}	4.0×10^{-4}	7.0×10^{-4}	5.1×10^{-4}
A_T, m s^{-1}	0.31	0.22	0.32	0.32
a_1, m s^{-1}	-0.15×10^{-4}	-0.28×10^{-4}	-1.0×10^{-4}	-0.04×10^{-4}
b_1, m s^{-1}	9.4×10^{-2}	1.5×10^{-2}	1.7×10^{-2}	0.18×10^{-2}
m	0.068	0.061	0.37	0.17
n'	0.26	0.30	0.18	0.20
r^2	0.99	0.99	0.99	0.99
χ^2	1.5×10^{-3}	7.9×10^{-3}	1.14×10^{-3}	0.79×10^{-3}

Figure 9. Normalized per cent difference between the predicted and measured gas transfer velocities, E_N, defined in (9) plotted versus bubble plume coverage, B_C, for evasion of CO_2, He, O_2, and SF_6 in cleaned (C) freshwater and for evasion of CO_2, He, and SF_6 in surfactant-influenced (SI) freshwater at a water temperature, T_W, of 293 K. The horizontal dashed lines show the experimental uncertainty ($\pm 1\sigma$) averaged over all k_L values. The data key is shown on the figure.
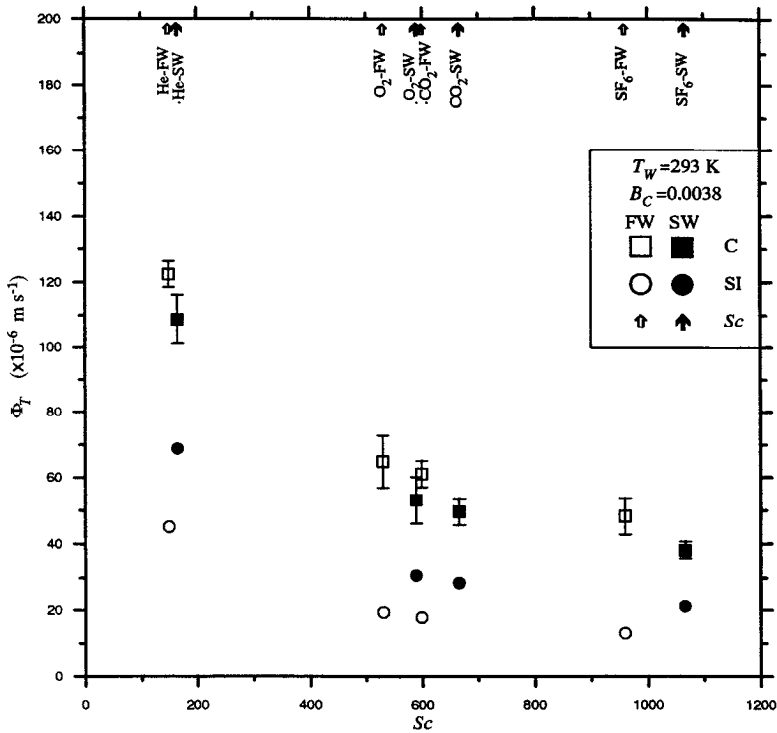
Figure 10. The portion of the total transfer due to turbulence processes, Φ_T, plotted versus Schmidt number, Sc. Φ_T was calculated using (5) and the coefficients in Table 4 for evasion of CO_2, He, O_2, and SF_6 in cleaned (C) and surfactant-influenced (SI) freshwater (FW) and seawater (SW). The fractional area bubble plume coverage, B_C, was 0.0038 and the water temperature, T_W, was 293 K. The error bars show the experimental uncertainty ($\pm 1\sigma$). The data key is shown on the figure.

where k_L (Predicted) is the predicted value and k_L (Measured) is the measured value. The data in Figure 9 show that the optimization provided estimates of the experimental data that were within the range of the typical experimental uncertainty. It is not clear why the optimization consistently underpredicted k_L for $B_C = 0.0010$ in both cleaned and SI freshwater.

Figure 10 shows Φ_T calculated for CO_2, He, O_2, and SF_6 at $B_C = 0.0038$ and $T_W = 293$ K using (5) and the coefficients in Table 4 for cleaned and SI freshwater and seawater plotted versus Sc. Comparing Φ_T for cleaned water, $\Phi_T(C)$, with Φ_T for SI water, $\Phi_T(SI)$, for a particular gas shows that the surfactant decreased Φ_T in both media. The decrease in $\Phi_T(SI)$ for freshwater was larger than the decrease for seawater even though the concentration of Triton X-100 was the same in both systems. This suggests that the surfactant had a larger effect in freshwater than in seawater. The reasons for this difference are not known at present.

In the absence of bubbles, it has been shown that k_L is proportional to the square root of

the turbulence velocity scale, Q (Brumley and Jirka, 1988). Furthermore, it was shown in Section 3a that the small-scale RMS velocity fluctuations were 20% larger in cleaned freshwater than in cleaned seawater. Assuming that these fluctuations gave a good estimate of Q and assuming that the hydrodynamics of turbulence-governed transfer are the same in freshwater and seawater (i.e., the slight change in Sc exponent from 0.5 to 0.56 from freshwater to seawater did not affect the dependence of Φ_T on Q), it would be expected that Φ_T in freshwater would be 10% larger than Φ_T in seawater. The data in Figure 10 show that $\Phi_T(C)$ for He in freshwater was 7% larger than $\Phi_T(C)$ for He in seawater. Similarly, $\Phi_T(C)$ for SF_6 in freshwater was 20% larger than the corresponding value for SF_6 in seawater. Given the experimental uncertainties in the underlying k_L values, both of these differences are consistent with the estimated change in Φ_T based on the PDA velocity measurements. (Note that because Sc for a gas changes slightly from freshwater to seawater, the $\Phi_T(C)$ values for seawater used in the above comparisons were calculated using Sc values for freshwater for the respective gases.)

Asher *et al.* (1996) showed that the nonlinear optimization procedure was accurately estimating $\Phi_T(C)$ and $\Phi_B(C)$ from the total measured seawater k_L values. This means that $\Phi_T(C)$ for seawater in Figure 10 could be used as a reference to determine whether $\Phi_T(C)$ for freshwater was accurate. The analysis in the preceding paragraph showed that the difference between $\Phi_T(C)$ for freshwater and seawater was consistent with the difference in the available estimates for Q. This suggests that $\Phi_T(C)$ for freshwater also was accurate, and more importantly because of the partitioning of k_L into its two components, if $\Phi_T(C)$ for freshwater was correct then $\Phi_B(C)$ must also be correct. Therefore, the coefficients listed in Table 4 for Φ_B can be used to examine the differences between bubble-mediated transfer in freshwater and seawater.

Figure 11 is $\Phi_B(C)$ and $\Phi_B(SI)$ plotted versus α for evasion of CO_2, He, O_2, and SF_6 in freshwater and seawater calculated for $B_C = 0.0038$ at $T_W = 293$ K using (6) and the coefficients in Table 4. In agreement with bubble-mediated gas transfer models, both $\Phi_B(C)$ and $\Phi_B(SI)$ for freshwater and seawater generally decreased as α increased. The exception to this trend was Φ_B for SF_6, which was caused by Φ_B being a function of both α and Sc. This effect is discussed in detail below.

Figure 11 shows that $\Phi_B(C)$ for freshwater was greater than $\Phi_B(C)$ for seawater. The modeling studies of Keeling (1993) and Woolf (1993) have shown that the bubble-mediated gas flux increases as the population of large bubbles increases. Because there were more large bubbles in freshwater than seawater (see Fig. 4), it follows that the bubble-mediated flux was larger in freshwater. In addition, the decrease in the concentration of small bubbles from seawater to freshwater decreased the overall dependence of $\Phi_B(C)$ on α (Keeling, 1993). This is why the largest increase in $\Phi_B(C)$ between seawater and freshwater was observed for CO_2.

Comparison of $\Phi_B(C)$ with $\Phi_B(SI)$ for seawater shows that the presence of the surfactant decreased Φ_B for the insoluble gases He, O_2, and SF_6, but had no effect on Φ_B for the more soluble gas CO_2. This was a consequence of the interplay between the effect of a surfactant
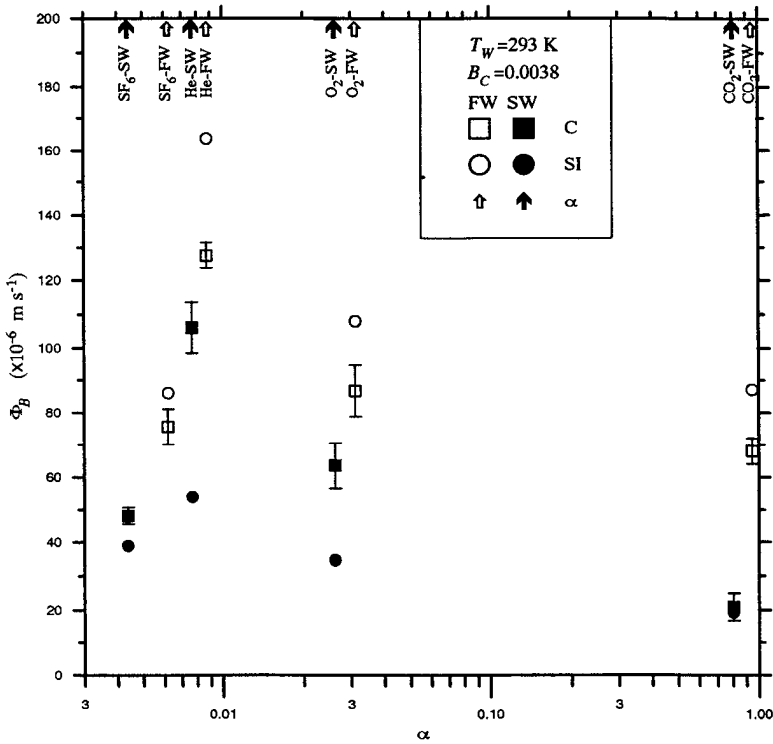
Figure 11. The portion of the total transfer due to bubble processes, Φ_B, plotted versus Ostwald solubility, α. Φ_B was calculated using (6) and the coefficients in Table 4 for evasion of CO_2, He, O_2, and SF_6 in cleaned (C) and surfactant-influenced (SI) freshwater (FW) and seawater (SW) at a fractional area bubble plume coverage, B_C, of 0.0038 and at a water temperature, T_W, of 293 K. The error bars show the experimental uncertainty ($\pm 1\sigma$). The data key is shown on the figure.

on the gas flux to an individual bubble and the relationship of solubility and bubble equilibration time with the gas flux to an individual bubble.

In general, the gas flux between a bubble and the surrounding water is a product of the transfer velocity of an individual bubble, κ_{bub}, and the bubble-water concentration difference. Because of the finite volume of a bubble, the gas in it equilibrates with the water on a finite time scale, τ_{eq}. This time scale can be written in terms of κ_{bub} and α as (Memery and Merlivat, 1985)

$$\tau_{eq} = \frac{4\pi r}{3\alpha\kappa_{bub}} \qquad (10)$$

where κ_{bub} is a function of Sc^{-n} and can be estimated using the formulae given by Memery and Merlivat (1985). Although the presence of a surfactant increases τ_{eq} by decreasing κ_{bub} (Clift *et al.*, 1978), τ_{eq} for a soluble gas may be short enough that the bubble still equilibrates. For example, a clean bubble with $r = 200$ μm at a starting depth of 0.25 m

rises to the surface in 6.3 s while τ_{eq} for CO_2 in the same bubble is 0.15 s. Therefore, CO_2 equilibrates with the surrounding water as the bubble rises to the surface. If the bubble is film-covered, $\tau_{eq} = 0.7$ s for CO_2 and its subsurface lifetime is 8.3 s, so it still has time to reach equilibrium. The net gas flux between an equilibrated bubble and the surrounding water is a function of the bubble volume and α, but independent of κ_{bub}. Therefore, because surfactants have no effect on α and because τ_{eq} is small for soluble gases and bubbles equilibrate, surfactants have little effect on Φ_B for a soluble gas such as CO_2. This effect was observed in the seawater data shown in Figure 11.

Surfactants affect Φ_B for an insoluble gas because τ_{eq} is large when α is small. For example, τ_{eq} for SF_6 in a 200-μm clean bubble is 28 s, far longer than the subsurface lifetime of 6.3 s. In this case the bubble does not equilibrate and the gas flux to it is a function of κ_{bub}. Because surfactants decrease κ_{bub} more than they increase the subsurface lifetime (Clift *et al.*, 1978), the bubble-mediated gas flux and Φ_B also decrease. This was observed experimentally in seawater with $\Phi_B(SI)$ for He, O_2, and SF_6 all being less than the corresponding value of $\Phi_B(C)$.

The explanation for the difference between $\Phi_B(C)$ and $\Phi_B(SI)$ in seawater should also have been applicable to Φ_B in freshwater. However, in freshwater $\Phi_B(SI)$ was larger than $\Phi_B(C)$, which is a reasonable result given the increase in $n(r)$ that occurred in freshwater when the surfactant was added. Figure 4 shows that $n(r)$ in SI freshwater was over a factor of ten larger than $n(r)$ in cleaned freshwater for 50 μm $< r <$ 500 μm. Because κ_{bub} decreased by no more than a factor of four between clean and SI bubbles (Memery and Merlivat, 1985), a ten-fold increase in the number of bubbles would have resulted in a larger total bubble-mediated gas flux, despite the decrease in κ_{bub}.

In freshwater and seawater, Φ_B for SF_6 was less than Φ_B for He and O_2 (see Fig. 11). At first glance, this suggests that bubble-mediated processes were less important for SF_6 than the other gases. However, the bubble-dependent gas flux was a function of both α and Sc, with the flux decreasing as Sc increased. Because SF_6 had the largest Sc of the gases shown, it had a relatively low Φ_B compared with the other gases. However, this does not mean that bubble-mediated processes were unimportant in the transfer of SF_6.

Figure 12 is a plot of the fraction of the total transfer velocity that was due to bubble-mediated processes, $\Phi_B/(\Phi_B + \Phi_T)$, calculated for the data in Figures 10 and 11. The data for cleaned and SI seawater show that the fraction of the total flux due to bubbles was larger for SF_6 than for any of the other gases, although the difference between SF_6 and O_2 is not statistically significant. Both data sets also show a general decrease in $\Phi_B/(\Phi_B + \Phi_T)$ as α increased. These observations are consistent with model results, which show that the importance of the bubble-mediated gas flux increases as α decreases (Memery and Merlivat, 1985; Woolf, 1993). The relatively low value of $\Phi_B/(\Phi_B + \Phi_T)$ for He was caused by the low Sc of He. Because Sc was small for He, Φ_T was large (see Fig. 10) and the relative fraction of the total flux due to bubbles decreased despite its large Φ_B (see Fig. 11).

Figure 12 shows that the relative importance of bubble-mediated transfer processes in
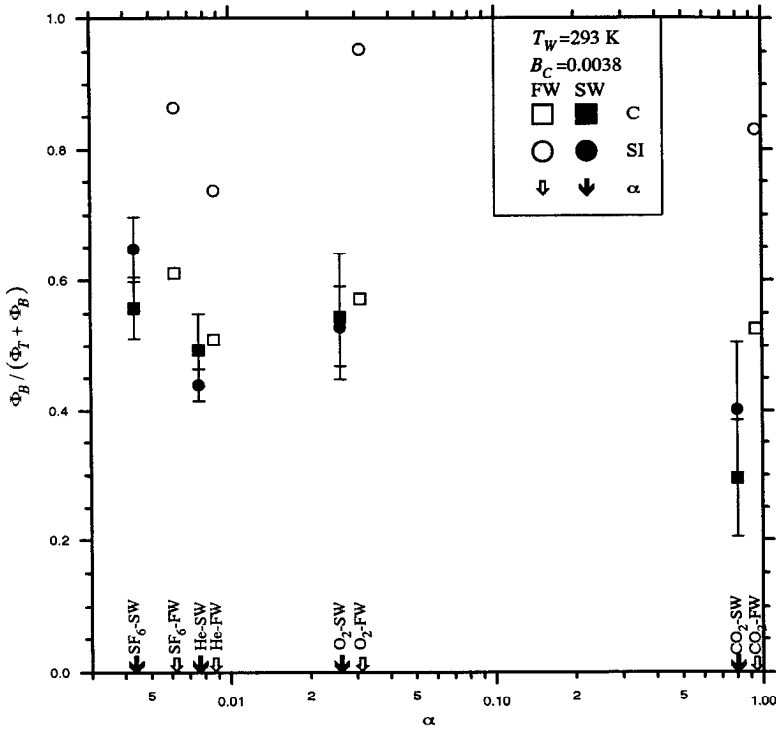
Figure 12. The fraction of the total transfer velocity that was due to bubble-mediated processes, $\Phi_B/(\Phi_B + \Phi_T)$, plotted versus Ostwald solubility, α, for evasion of CO_2, He, O_2, and SF_6 in cleaned (C) and surfactant-influenced (SI) freshwater (FW) and seawater (SW). The turbulence-mediated transfer coefficient, Φ_T, and the bubble-mediated transfer coefficient, Φ_B, were calculated using (5) and (6), respectively, and the coefficients listed in Table 4 for each water type and surfactant condition at a fractional area bubble plume coverage, B_C, of 0.0038 and at a water temperature, T_W, of 293 K. The error bars show the typical experimental uncertainty ($\pm 1\sigma$). The data key is shown on the figure.

cleaned freshwater was relatively insensitive to changes in α. This insensitivity resulted from the increased concentration of bubbles with $r > 500 \, \mu m$ and decrease in the concentration of small bubbles (Keeling, 1993).

In seawater, $\Phi_T(SI)$ and $\Phi_B(SI)$ were less than their respective values for the cleaned case. Coincidentally, both decreased by approximately the same relative amount so that there was little significant change in $\Phi_B/(\Phi_B + \Phi_T)$ between cleaned and SI seawater. In freshwater however, $\Phi_B(SI)/(\Phi_B(SI) + \Phi_T(SI))$ for a particular gas increased compared to the corresponding value in the cleaned media. Figure 10 shows that the addition of surfactant decreased Φ_T while Figure 11 shows that adding surfactant increased Φ_B. The opposite effect of the surfactant on Φ_B and Φ_T explains why $\Phi_B/(\Phi_B + \Phi_T)$ was so large in SI freshwater.

The dependence of Φ_B on both Sc and α for cleaned seawater is more clearly seen in the
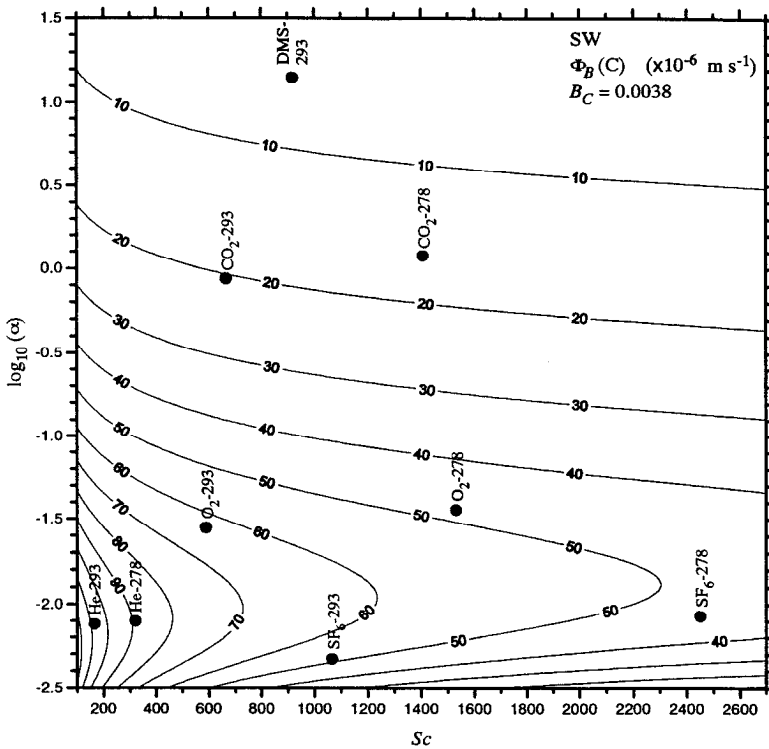
Figure 13. Contour plot of the portion of the total transfer velocity that is due to bubble-mediated processes, Φ_B, for evasion in cleaned seawater as a function of Schmidt number, Sc, and logarithm of the Ostwald solubility, α. Φ_B was calculated using (6) and the cleaned seawater coefficients listed in Table 4 for a fractional area bubble plume coverage, B_C, of 0.0038 and a water temperature, T_W, of 293 K. Contour intervals are in units of 10×10^{-6} m s^{-1}. Also shown are the seawater data that Asher *et al.* (1996) used to determine the seawater coefficients in Table 4.

contour plot in Figure 13. When solubility was constant (horizontal lines in Fig. 13), Φ_B decreased as Sc increased (i.e., decreasing diffusivity) due to the dependence of the bubble-mediated gas flux on Sc^{-n} through κ_{bub}. However, for larger values of $\log_{10}(\alpha)$ there was little dependence of Φ_B on Sc for constant α because the bubbles equilibrated. In this case, the bubble-mediated gas flux was independent of diffusivity.

At constant Sc (vertical lines in Figs. 13), Φ_B increased with decreasing solubility for $\log_{10}(\alpha)$ in the range of 1.5 to -2. This agrees with the results of modeling studies that show that the bubble-mediated gas flux increases as solubility decreases (Memery and Merlivat, 1985; Woolf, 1993). However, in contrast to the model predictions Φ_B reached a maximum value as $\log_{10}(\alpha)$ decreased to approximately -2 (where the exact value at maximum was a function of Sc) and further decreases in $\log_{10}(\alpha)$ caused Φ_B to decrease. This decrease in Φ_B for small values of α is most likely an artifact caused by extrapolating the parameterization of Φ_B beyond the range of the fitted data. In Figure 13, for all gases

studied (with the exception of SF_6 at $T_W = 293$ K, which is discussed in detail below), Φ_B at the Sc of that particular gas decreased as α increased. This shows that in the range of the fitted data, the dependence of Φ_B defined by the parameterization behaved similarly to fluxes calculated using numerical models of bubble-mediated gas exchange.

In the case of SF_6, the parameterization for Φ_B predicts that a gas with a slightly higher solubility but the same Sc would have a larger bubble-mediated transfer velocity. However, calculating the gas flux to an individual bubble as described by Woolf (1993) shows that when Sc is constant the flux, and therefore Φ_B, should decrease as solubility increases. Although this disagreement can not be resolved using the current data set, it is likely that behavior of the parameterization for Φ_B differs from model predictions due to the combined interaction of the nonlinear optimization with the experimental uncertainty in the fitted data and the behavior of Φ_B with respect to α and Sc that is predicted by theoretical considerations.

This can be more clearly explained in terms of the gas flux to an individual bubble. First, assume that the plume was mono-disperse and consisted of bubbles with constant r generated at the same depth. In this case, the number of moles of gas transferred to an individual bubble, Δn, will be directly proportional to Φ_B. Δn is given by (Woolf, 1993)

$$\Delta n = \left[1 - \exp\left(-\frac{\tau_{bub}}{\tau_{eq}}\right)\right] (n_0 - n_E) \tag{11}$$

where n_0 is the initial number of moles of transferring gas in the bubble and n_E is the number of moles of the gas in the bubble when it has reached equilibrium. The subsurface lifetime of each bubble, τ_{bub}, is constant and equal to the depth divided by the rise velocity. Because τ_{bub} is constant and because τ_{eq} and n_E can be written explicitly in terms of Sc and α, the functionality of Δn and therefore Φ_B can be determined analytically.

Woolf (1993) has shown that when r and the gas concentration in the aqueous phase are constant, n_E is proportional to α^{-1}. Furthermore, (10) and the relations for κ_{bub} in Memery and Merlivat (1985) show that τ_{eq} is proportional to $\alpha^{-1} Sc^n$. Therefore, when Sc is constant Δn and Φ_B increase as α decreases. However, the rate of increase of Δn with respect to the rate of decrease in α is not constant. Figure 14 is a contour plot of Δn calculated using (11) for a dirty bubble with $r = 100$ μm rising from an initial depth of 0.25 m. For a dirty 100-μm bubble, $\tau_{bub} = 21$ s (Woolf and Thorpe, 1991) and $\kappa_{bub} = 13.7 \times Sc^{-2/3}$ cm s^{-1} (Memery and Merlivat, 1985).

For $\log_{10}(\alpha) > -0.5$, Figure 14 shows that Δn is independent of α and Sc, which implies that for $\alpha > 0.3$ a 100-μm bubble equilibrates. In terms of the nonlinear optimization, this range was spanned by CO_2 at $T_W = 278$ K and 293 K and DMS at $T_W = 293$ K. Their Sc and α values are arranged in a triangle pattern, defining the plane where Δn and Φ_B are constant. Because these three points are not collinear, the nonlinear optimization procedure used to estimate the coefficients in Table 4 performed well even in the presence of a small level of experimental noise. However, for $\log_{10}(\alpha) < -2$ all of the available data points are nearly collinear with respect to α. Unfortunately, in this range there is little increase in Δn
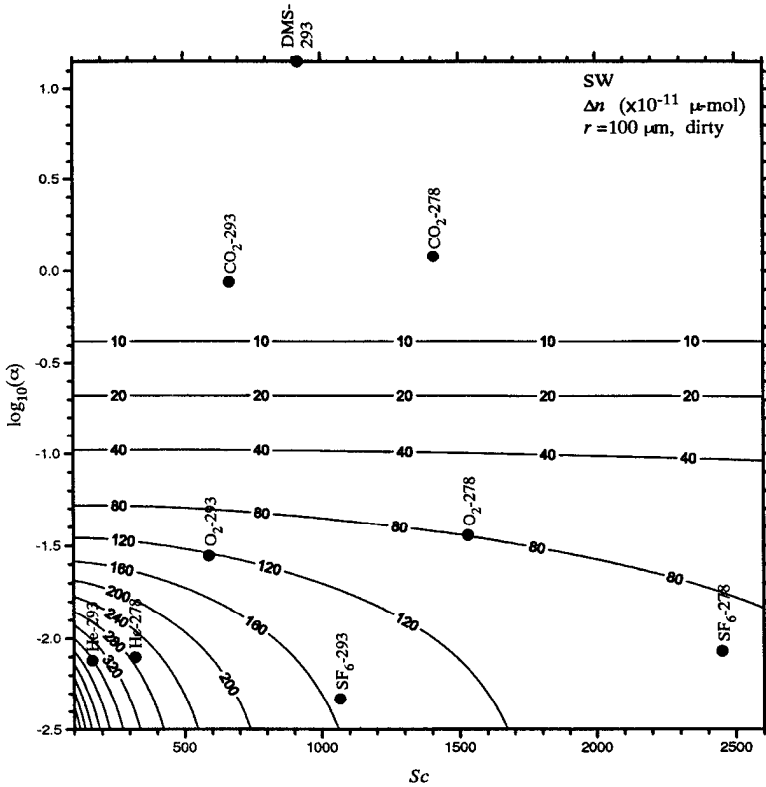
Figure 14. Contour plot of the total number of moles of gas taken up by a bubble, Δn, as a function of Schmidt number, Sc, and logarithm of the Ostwald solubility, α. Δn was calculated using (11) for a dirty bubble with a radius of 100 μm rising from a depth of 0.25 m at a water temperature, T_W, of 293 K. The initial concentration of the transferring gas in the bubble was zero and the concentration of gas in the surrounding water was 10 μ-mol m^{-3}. Contour intervals are in units of 1 × 10^{-11} μ-mol. Also shown are the seawater data that Asher *et al.* (1996) used to determine the seawater coefficients in Table 4.

with decreasing α (i.e., the curves of constant Δn become vertical). Due to the small change in Δn and the collinearity of the available data points with respect to α, it was difficult for the nonlinear optimization to correctly describe the behavior of Φ_B at small α beyond the limits of the fitted data.

The decrease in Φ_B for SF$_6$ and gases with lower solubility does not imply that the empirical parameterizations determined in this paper are invalid. In the regions bounded by the experimental data points, the contour lines for Φ_B in Figure 13 have a similar shape to the contour lines for Δn in Figure 14. However, it would be unwise to use (4) and the coefficients in Table 4 to predict Φ_B for gases whose α and Sc values lie outside of the experimental data points. However, this limitation does not severely restrict the use of (4) because the ranges in Sc and α spanned by the data cover most gases of environmental interest.
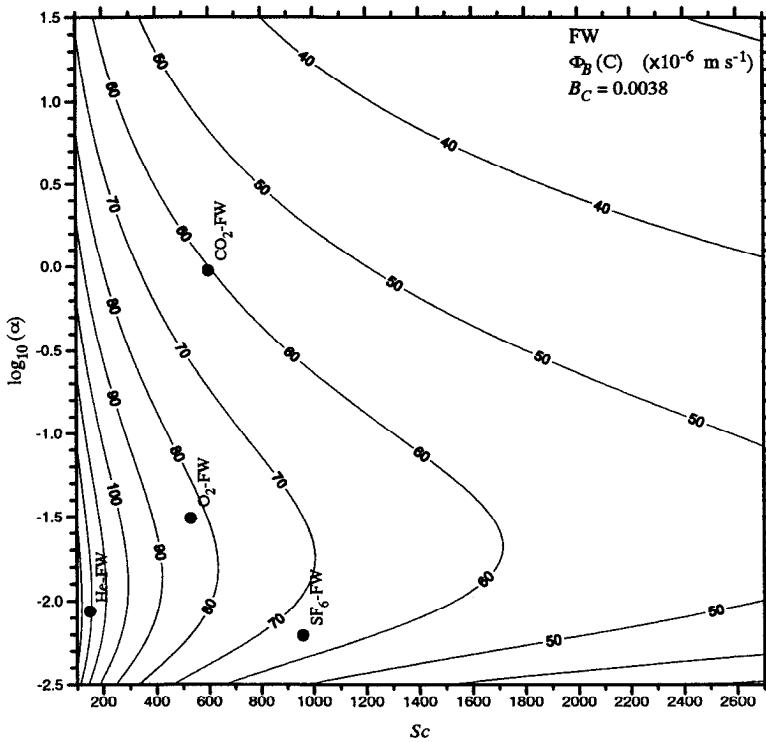
Figure 15. Contour plot of the portion of the total transfer velocity that is due to bubble-mediated processes, Φ_B, for evasion in cleaned freshwater as a function of Schmidt number, Sc, and logarithm of the Ostwald solubility, α. Φ_B was calculated using (6) and the cleaned freshwater coefficients listed in Table 4 for a fractional area bubble plume coverage, B_C, of 0.0038 and a water temperature, T_W, of 293 K. Contour intervals are in units of 10×10^{-6} m s^{-1}. Also shown are the freshwater data used to determine the freshwater coefficients in Table 4.

For comparison purposes, Figure 15 shows a contour plot of Φ_B for evasion in cleaned freshwater. The shape of the contours for freshwater are similar to the contours of Φ_B for seawater in Figure 13. However, Φ_B in freshwater has a much stronger dependence on Sc at large α than Φ_B in seawater and Φ_B is less sensitive to changes in α. These differences are consistent with the effect that the increased population of large bubbles and decreased population of small bubbles in freshwater would have on bubble-mediated transfer (Keeling, 1993).

A final word is necessary on the possible effects that miscalibration of B_C in SI freshwater would have on the above discussion. First, it should be stressed that this problem has no impact on the conclusions or analyses regarding the data from cleaned freshwater, cleaned seawater, or SI seawater. In these three cases it is reasonably certain that B_C was accurate. Underestimation of B_C would only have been a problem for the SI freshwater results and would have caused the transfer velocities to be lower at a given value of B_C. Assuming B_C was a factor of two too high means that the values for Φ_T and Φ_B

in Figures 10 and 11 were also approximately a factor of two too high (i.e., recalculating the coefficients using the new values for B_C does not affect the fit). This shows that Φ_B in SI freshwater would have been lower than Φ_B in cleaned freshwater, in similarity with the seawater results. Φ_B in SI freshwater would still be higher than Φ_B in SI seawater, as might be expected based on the higher concentration of bubbles in SI freshwater.

5. Conclusions

Overall, k_L values measured in either cleaned freshwater, cleaned seawater, SI freshwater or SI seawater were linearly correlated with B_C. This allowed k_L to be partitioned into a bubble- and a turbulence-mediated fraction. Because of the increased concentration of larger bubbles, bubble-mediated gas fluxes in cleaned freshwater were higher than the fluxes in cleaned seawater. This was especially true as the solubility of the gas increased. Additionally, the freshwater bubble-mediated transfer velocity showed less dependence on solubility than the bubble-mediated transfer velocity in seawater. The difference between the turbulence-mediated transfer velocities in both of the cleaned-water systems was consistent with the estimated difference in the turbulence.

The addition of a soluble surfactant decreased k_L in both freshwater and seawater, but the surfactant had a much larger effect on k_L in seawater. This was caused by the difference between the response of the bubble population in freshwater and seawater when surfactant was added. In seawater, the surfactant caused little change in the concentration of bubbles. However, there was a large increase in the bubble concentration when surfactant was added to freshwater, causing an increase in the bubble-mediated gas flux. The increase in the bubble-mediated gas flux in SI freshwater partially offset the decrease in the turbulence-mediated gas flux.

The results presented here show that caution should be used in applying relationships developed using results from freshwater bubble-mediated gas exchange measurements to seawater systems and *vice versa*. Because of the difference in bubble populations, parameterizations developed using data collected in freshwater will overestimate the bubble gas flux in seawater, especially for a soluble gas such as CO_2. These results also demonstrate the need for proper control of surfactants when conducting bubble-mediated exchange experiments. Figure 11 shows that the effect of a surfactant on bubble-mediated transfer in seawater can be insignificant for a soluble gas or the effect can be very large for an insoluble gas. However, in freshwater the presence of a surfactant increased the bubble-mediated gas flux by up to 40% regardless of solubility. Therefore, it would be difficult to relate laboratory measurements made under unknown bubble and surfactant conditions to bubble-mediated transfer under oceanic conditions. Accurate relation of bubble gas transfer measurements made in different laboratory systems will require knowledge of the bubble populations.

Finally, the parameterizations developed here and the coefficients listed in Table 4 are only applicable to evasion when the gas concentration is far from equilibrium. Due to the asymmetry between evasion and invasion for bubble processes, these relations should not

be used to estimate transfer velocities for invasion. Similarly, these parameterizations should not be used to estimate evasive transfer velocities when the air-water concentration difference is near equilibrium. However, it has been shown that (4) does provide an accurate partitioning of k_L in the WST into the turbulence and bubble fractions. Therefore, it is likely that if the differences between freshwater and seawater bubble plumes under environmental conditions are similar to the differences seen here, gas exchange results measured in the two media would have similar behavior as found here.

APPENDIX

List of notations.

a_1 constant for parameterizing k_B as defined in (3), m s^{-1}.

A proportionality constant relating k_L to Sc^{-n}, m s^{-1}.

A_M proportionality constant relating k_M to Sc^{-n}, m s^{-1}.

A_T proportionality constant relating k_T to Sc^{-n}, m s^{-1}.

b_1 constant for parameterizing k_B as defined in (3), m s^{-1}.

B_C fractional area bubble plume coverage.

D molecular diffusivity, m^2 s^{-1}.

E_N normalized per cent difference between predicted and measured k_L values defined in (9).

F air-water flux, mol m^{-2} s^{-1}.

FW   freshwater.

k_B bubble-mediated transfer velocity, m s^{-1}.

k_L total transfer velocity, m s^{-1}.

k_M nonwhitecap-generated turbulence transfer velocity, m s^{-1}.

k_T whitecap-generated turbulence transfer velocity, m s^{-1}.

m exponent for α used in parameterizing k_B, defined in (3).

n exponent for Sc defined in (1).

n' exponent for Sc used in parameterizing k_B, defined in (3).

n_0 initial number of moles of gas in bubble, mol.

n_E number of moles of gas in bubble at equilibrium, mol.

$p\text{CO}_2$ partial pressure of CO_2, atm.

PDA   phase-Doppler anemometer.

Q turbulence velocity scale, m s^{-1}.

r bubble radius, μm.

r^2 coefficient of determination.

Sc Schmidt number (equal to ν/D).

SI   surfactant-influenced.

SW   seawater.

t_A time elapsed after creation of bubble plume, s.

t_B time between simulated whitecaps, s.

t_P lifetime of actively entraining, or Stage A, bubble plume, s.

T_W water temperature, K.

v_B bubble rise velocity, cm s^{-1}.

v_z vertical bubble velocity (positive in upwards direction), m s^{-1}.

V_F fill volume of tipping bucket, m^3.

WST   whitecap simulation tank.

z depth, m.

α Ostwald solubility.

ΔC air-water concentration difference, mol m^{-3}.

Δn total number of moles of gas transferred to bubble, mol.

κ_{bub} transfer velocity of an individual bubble, m s^{-1}.

ν kinematic viscosity, m^2 s^{-1}.

σ standard deviation.

τ_{bub} subsurface bubble lifetime, s.

τ_{eq} bubble equilibration time, s.

$\phi(t_A)$ instantaneous fractional area bubble plume coverage.

Φ_B portion of k_L due to bubble processes defined in (6), m s^{-1}.

Φ_T portion of k_L due to turbulence processes defined in (5), m s^{-1}.

χ^2 chi-square parameter defined in (8).

REFERENCES

Asher, W. E. and P. J. Farley. 1995. Phase-Doppler anemometer measurement of bubble concentrations in laboratory-simulated breaking waves. J. Geophys. Res., *100,* 7045–7056.

Asher, W. E., L. M. Karle, B. J. Higgins, P. J. Farley, I. S. Leifer and E. C. Monahan. 1996. The influence of bubble plumes on air-seawater gas transfer velocities. J. Geophys. Res., *101,* 12,027–12,041.

Asher, W., L. Karle, B. Higgins, P. Farley, C. Sherwood, W. Gardiner, R. Wanninkhof, H. Chen, T. Lantry, M. Steckley, E. Monahan, Q. Wang and P. Smith. 1995. Measurement of gas transfer, whitecap coverage, and brightness temperature in a surf pool: An overview of WABEX-93, *in* Air-Water Gas Transfer, B. Jähne and E. C. Monahan, eds., Aeon Verlag, Heidelberg, 205–216.

Asher, W. E. and R. Wanninkhof. 1997. Transient tracers and air-sea gas exchange. J. Geophys. Res., (in press).

Broecker, H. C. and W. Siems. 1984. The role of bubbles for gas transfer from water to air at higher wind speeds, *in* Gas Transfer at Water Surfaces, W. Brutsaert and G. H. Jirka, eds., Reidel, Dordrecht, 229–236.

Brumley, B. H. and G. H. Jirka. 1988. Air-water transfer of slightly soluble gases: turbulence, interfacial processes and conceptual models. Physicochem. Hydrodyn., *10,* 295–319.

Clift, R., J. R. Grace and M. E. Weber. 1978. Bubbles, Drops, and Particles, Academic Press, NY, 380 pp.

DOE, 1994. Handbook of Methods for the Analysis of the Various Parameters of the Carbon Dioxide System in Sea Water; Version 2, Oak Ridge National Laboratory/Carbon Dioxide Information and Analysis Center Publication 74, A. G. Dickson and C. Goyet, eds., 154 pp.

Haines, M. A. and B. D. Johnson. 1995. Injected bubble populations in seawater and freshwater measured by a photographic method. J. Geophys. Res., *100*, 7057–7069.

Hsiao, L., H. N. Dunning and P. B. Lorenz. 1956. Critical micelle concentrations of polyoxyethylated nonionic detergents. J. Phys. Chem., *60*, 657–660.

Jähne, B., T. Wais and M. Barabas. 1984. A new optical bubble measuring device; a simple model for bubble contribution to gas exchange, *in* Gas Transfer at Water Surfaces, W. Brutsaert and G. H. Jirka, eds., Reidel, Dordrecht, 237–246.

Keeling, R. F. 1993. On the role of large bubbles in air-sea gas exchange and supersaturation in the ocean. J. Mar. Res., *51*, 237–271.

Lange, H. and P. Jeschke. 1987. Surface monolayers, *in* Nonionic Surfactants: Physical Chemistry, M. J. Schick, ed., M. Dekker, New York, 1–44.

Memery, L. and L. Merlivat. 1985. Modeling of the gas flux through bubbles at the air-water interface. Tellus, *37B*, 272–285.

Monahan, E. C. 1989. From the laboratory tank to the global ocean, *in* Climate and Health Implications of Bubble-Mediated Sea-Air Exchange, E. C. Monahan and M. A. Van Patten, eds., Connecticut Sea Grant College Program, Groton, 265–301.

Monahan, E. C. and C. R. Zietlow. 1969. Laboratory comparisons of fresh-water and salt-water whitecaps. J. Geophys. Res., *74*, 6961–6966.

Reid, R. C., J. M. Prausnitz and B. E. Poling. 1987. The Properties of Gases and Liquids, 4th ed, McGraw-Hill, NY, 741 pp.

Shatkay, M. and D. Ronen. 1992. Bubble populations and gas exchange in hypersaline solutions: A preliminary study. J. Geophys. Res., *97*, 7361–7372.

Wanninkhof, R. 1992. Relationship between wind speed and gas exchange over the ocean. J. Geophys. Res., *97*, 7373–7382.

Wanninkhof, R., W. E. Asher and E. C. Monahan. 1995. The influence of bubbles on air-water gas exchange: Results from gas transfer measurements during WABEX-93, *in* Air-Water Gas Transfer, B. Jähne and E. C. Monahan, eds., Aeon Verlag, Hanau, 239–254.

Wanninkhof, R., J. R. Ledwell and A. J. Watson. 1991. Analysis of sulfur hexafluoride in seawater. J. Geophys. Res., *96*, 8733–8740.

Woolf, D. K. 1993. Bubbles and the air-sea transfer velocity of gases. Atmos.-Ocean, *31*, 517–540.

—— 1997. The role of bubbles in gas exchange, *in* The Sea Surface and Global Change, R. A. Duce and P. S. Liss, eds., Cambridge University Press, London. 173–205.

Woolf, D. K. and S. Thorpe. 1991. Bubbles and the air-sea exchange of gases in near-saturation conditions. J. Mar. Res., *49*, 435–466.